Heterogeneous Catalysis

DOI: 10.1002/anie.200904688

Hydrogen Diffusion into Palladium Nanoparticles: Pivotal Promotion by Carbon**

Konstantin M. Neyman and Swetlana Schauermann**

Activated diffusion of hydrogen into the subsurface region of metal nanoparticles is the central elementary step in many technically relevant processes, such as storage, separation and detection of hydrogen, development of switchable mirrors, and fuel cells. In the field of heterogeneous catalysis, involvement of subsurface hydrogen species in the hydrogenation of the olefinic double bonds is a subject of a long-standing discussion.[1–3] Recently, by employing hydrogen depth profiling with nuclear reaction analysis (NRA) and transient molecular beam experiments on model supported palladium nanoparticles (PdNPs), the presence of subsurface hydrogen atoms has been proven to be crucial for hydrogenation of 2-butene.[4] A striking observation of that study was that persistent hydrogenation catalytic activity can be achieved only in the presence of small amount of carbonaceous species,[4,5] a phenomenon for which the underlying microscopic mechanisms have not yet been revealed. It has been suggested that the promoting effect by co-deposited carbon is due to facilitated diffusion of hydrogen atoms into the subsurface state that governs hydrogenation activity.[4] Two microscopic-scale mechanisms have been invoked to rationalize a conceivable lowering of the activation barrier for hydrogen diffusion into the subsurface in the presence of deposited carbon: 1) a weakening of the binding of hydrogen on the surface and 2) local elongation of Pd–Pd bonds, rendering the surface more permeable to hydrogen.

Herein, we use computational studies to investigate the microscopic origin of the carbon-assisted subsurface diffusion of hydrogen atoms on Pd(111) terraces. Particular emphasis is placed on exploring the role of carbon-induced expansion of the palladium lattice in hydrogen subsurface diffusion, which is addressed by comparison of the atomically flexible (111) facets of PdNPs with an extended laterally stiff Pd(111) surface. Deposited carbon can dramatically enhance the hydrogen diffusion rate into the subsurface region of PdNPs, which is mainly due to local elongation of Pd–Pd bonds and a concomitant lowering of the diffusion barrier. This change may account for the unusual promotion of sustained hydrogenation activity that was experimentally observed. In contrast, the lateral rigidity of the extended Pd(111) surface is predicted to hinder the promotion of subsurface hydrogen diffusion by deposited carbon atoms.

Figure 1 shows the production rate of [D_2]butane resulting from the reaction of *cis*-2-butene with D_2 over an initially clean and a carbon-containing palladium-supported model catalyst. PdNPs of about 7 nm in size were prepared on a plain

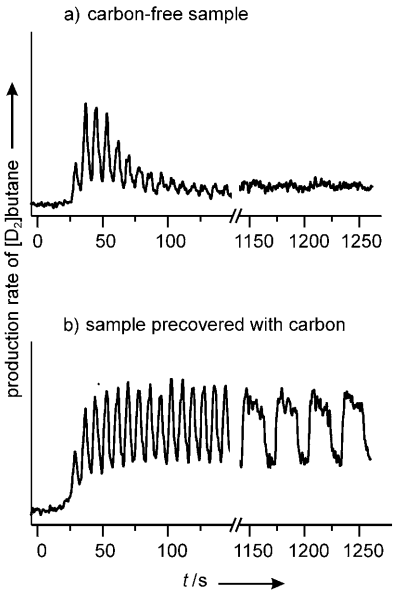

Figure 1. The hydrogenation reaction rate of *cis*-2-butene at 260 K over initially D_2-saturated clean (a) and carbon-precovered (b) model catalysts Pd/Fe_3O_4/Pt(111).

Fe_3O_4/Pt(111) film using a well-established procedure.[6] The carbonaceous species on PdNPs were prepared by annealing co-adsorbed *cis*-2-butene and deuterium to 485 K,[5] upon which essentially complete dehydrogenation of olefin was revealed both by temperature-programmed desorption (TPD) and infrared reflection absorption spectroscopy (IRAS). For reactivity measurements, the catalyst was first pre-exposed to a continuous D_2 beam to saturate the particles. A sequence of *cis*-2-butene pulses was then applied using an independent beam source along with the continuous D_2 exposure. On the pristine PdNPs (Figure 1 a), the initial period of high hydrogenation activity on deuterium-saturated catalyst is followed by a decrease of the reaction rate to zero

[*] Prof. Dr. K. M. Neyman
Institució Catalana de Recerca i Estudis Avançats (ICREA)
Pg. Lluís Companys, 23, 08010 Barcelona (Spain)
and
Departament de Química Física and Institut de Química Teòrica i Computacional (IQTCUB), Universitat de Barcelona
c/Martí i Franquès 1, 08028 Barcelona (Spain)
E-mail: konstantin.neyman@icrea.es
Dr. S. Schauermann
Fritz-Haber-Institut der Max-Planck-Gesellschaft
Faradayweg 4–6, 14195 Berlin (Germany)
E-mail: schauermann@fhi-berlin.mpg.de

[**] Support by the Spanish MICINN (grants FIS2008-02238, HA2006-0102) and EU (COST-D41) is gratefully acknowledged. The authors thank Prof. H.-J. Freund and Dr. M. Wilde for valuable discussions.

under steady-state conditions. Remarkably, carbon deposition prevents the suppression of hydrogenation in the steady state and results in persistent hydrogenation activity at the initially high level (Figure 1b). Deposited carbon modifies only a small fraction of the surface and, according to spectroscopic[5] and calculated[7] results, predominantly occupies the edge sites of the PdNPs, where essentially non-activated subsurface diffusion of atomic carbon has been predicted theoretically.[8]

The microscopic reasons for the decreased hydrogenation activity on the clean catalyst could be deduced from the combination of hydrogen depth profiling by NRA and transient molecular beam experiments carried out at different H_2/D_2 pressures.[4] The initially high hydrogenation rate on clean PdNPs was assigned to subsurface deuterium atoms present in PdNPs directly following saturation with the D_2 beam, but their concentration cannot be maintained at the initially high level under steady-state conditions. This observation is most likely a consequence of the competition between an activated process of H(D) subsurface diffusion and the H(D) consumption in the H/D exchange reaction of *cis*-2-butene. A conceivable explanation for the sustained hydrogenation activity of carbon-containing PdNPs is facilitated hydrogen diffusion that enables replenishing the subsurface reservoir under steady-state conditions. It has been proposed that carbon may decrease the activation barrier for the subsurface H(D) diffusion, thus promoting persistent hydrogenation.[4]

To examine this hypothesis, we performed density-functional calculations on model cuboctahedral Pd_{79} nanoparticles, which were shown to be representative for realistic description of surface interactions present on larger PdNPs experimentally studied in model catalysts,[9,10] especially for sites near particle edges. Comparison with Pd(111) slab models consisting of the surface unit cell (3 × 3) and six atomic layers of Pd, namely Pd(111)9 × 6 L, has been made to clarify importance of the mobility of surface palladium atoms for subsurface diffusion of adsorbed hydrogen.

At a low-coverage, $\theta_H \rightarrow 0$, where one hydrogen atom interacts with the central *fcc* site of a (111) facet of the Pd_{79} particle, we calculated hydrogen in the octahedral subsurface (oss) position just beneath the fcc surface (H^{oss}) to be less stable than the surface H^{fcc}, by about 30 kJ mol^{-1} (Table 1). On Pd(111), the H^{fcc} species are further stabilized relative to the H^{oss} species, and the subsurface diffusion barrier drastically increases by 17 kJ mol^{-1} relative to Pd_{79}.

Figure 2 shows Pd_{79} models that represent more realistic experimentally investigated[4] case of subsurface hydrogen diffusion on the hydrogen-saturated surface ($\theta_H \approx 1$ ML). Six

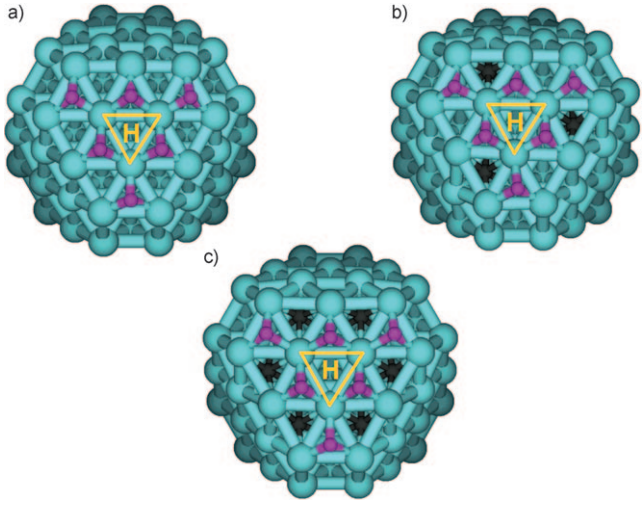

Figure 2. Pd_{79} nanoparticle with six H^{hcp} atoms (a) and those with subsurface C atoms, $Pd_{79}C_3$ (b) and $Pd_{79}C_6$ (c). The triangles indicate the Pd_3 moiety through which we studied subsurface diffusion of the central atom H_{fcc}. Pd turquoise, C black, H^{hcp} pink, H^{fcc}/H^{oss} yellow.

H^{hcp} atoms were placed on the (111) facet and an additional H atom was positioned in the central fcc site. For this H^{fcc} atom, the binding energies and the activation barriers for diffusion to the subsurface oss position right below the surface adsorption site were calculated both on the pristine (Figure 2a) and carbon-containing Pd_{79} (Figure 2b and 2c). On the pristine nanoparticle, $H^{hcp}{}_6Pd_{79}$, the subsurface H^{oss} atom was almost isoenergetic with the surface H^{fcc} atom ($E_{abs}(H^{oss}) = -206$ kJ mol^{-1} vs. $E_{ads}(H^{fcc}) = -201$ kJ mol^{-1}) and the activation barrier for hydrogen subsurface diffusion was computed to be 17 kJ mol^{-1}. Upon addition of three subsurface carbon atoms (Figure 2b), the subsurface H^{oss} atom became clearly energetically favored over the surface atom ($E_{abs}(H^{oss}) = -204$ kJ mol^{-1} vs. $E_{ads}(H^{fcc}) = -185$ kJ mol^{-1}), so that the thermodynamic driving force could be identified for hydrogen subsurface diffusion, which mainly arises from weaker adsorption interactions of the surface hydrogen atom. Moreover, the activation barrier for this process, about 2 kJ mol^{-1}, is nearly eliminated. At a typical reaction temperature of 250–260 K, such a decrease of the activation barrier corresponds to an increase of the hydrogen subsurface diffusion rate by three orders of magnitude relative to the carbon-free particle. Favoring subsurface hydrogen is even more pronounced on the substrate Pd_{79} containing six carbon atoms (Figure 2c). In this case, it was not possible to stabilize an hydrogen atom in the surface fcc position. Instead, a spontaneous

Table 1: Energies of H adsorbed on and absorbed in the subsurface of Pd_{79} and the subsurface diffusion barrier in the central Pd_3 site (see Figure 2).[a]

	Pd_{79}	$H^{hcp}{}_6Pd_{79}$	$H^{hcp}{}_6Pd_{79}C_3$	$H^{hcp}{}_6Pd_{79}C_6$
$E_{ads}(H^{fcc})$ [kJ mol^{-1}]	−238 (−243)	−201 (−155)	−185 (−136)	unstable
$\Delta E^{\ddagger}$ [kJ mol^{-1}]	29 (46)	17 (20)	2 (11)	–
$E_{abs}(H^{oss})$ [kJ mol^{-1}]	−209 (−202)	−206 (−199)	−204 (−174)	−187
d_{bare} [pm][b,c]	263 (275)	271 (275)	282 (275)	295
d_{ads} [pm][b]	269 (280)	275 (277)	288 (277)	unstable
$d^{\ddagger}$ [pm][b]	286 (291)	289 (288)	296 (288)	–
d_{abs} [pm][b]	268 (285)	272 (277)	285 (277)	299

[a] Values in parentheses are for the slab models Pd(111)9 × 6 L in which monolayer coverage has been considered to be nine H^{hcp} atoms per unit cell instead of six H^{hcp} atoms on a (111) facet of a Pd_{79} particle. [b] Pd–Pd distances in the Pd_3 moiety. [c] Models without the central H^{fcc}/H^{oss} atoms.

migration into the subsurface oss position took place when we attempted to optimize the geometry of the system.

This trend can be understood in terms of carbon-induced palladium cluster distortions assisting in the subsurface hydrogen diffusion. For that, we analyzed the average Pd–Pd bond lengths d within the surface central Pd_3 moiety nearest to the diffusion site (Table 1), labeled by a yellow triangle in Figure 2. On carbon-free Pd_{79}, the $H^{hcp}{}_6$ overlayer extends the Pd–Pd distance d_{bare} by 8 pm. Three and six carbon atoms added to $H^{hcp}{}_6Pd_{79}$ further increase d_{bare} by 11 and 24 pm, respectively, pointing to a high ability of carbon to expand the palladium lattice.

There is a distinct correlation between the activation barrier $\Delta E^{\neq}$ for subsurface H diffusion and the Pd–Pd distance $d^{\neq}$ in the transition state (TS): the most-expanded Pd_3 moiety in the carbon-containing $H^{hcp}{}_6Pd_{79}C_3$ cluster, having $d^{\neq} = 296$ pm, corresponds to the lowest (essentially zero) activation energy, whilst $\Delta E^{\neq}$ noticeably increases for the less-expanded configurations without carbon ($\Delta E^{\neq} = 17\ kJ\,mol^{-1}$, $d^{\neq} = 289$ pm) and without $H^{hcp}{}_6$ ($\Delta E^{\neq} = 29\ kJ\,mol^{-1}$, $d^{\neq} = 286$ pm). This result shows that the low-barrier TS requires space in the form of a large Pd_3 opening, and nearby carbon atoms efficiently assist in elongation of the Pd–Pd bonds; the hydrogen overlayer was found to act in a similar way but to a lesser extent. In the $H^{hcp}{}_6Pd_{79}C_6$ model with six carbon atoms, the initial Pd_3 opening $d_{bare} = 295$ pm is already almost as large as the $d^{\neq}$ found for the lowest-energy TS, and therefore the subsurface diffusion of hydrogen occurs spontaneously. This result corroborates our finding on a crucial role of carbon-induced local lattice expansion of PdNPs with rather flexible Pd–Pd bonds in facilitation of hydrogen subsurface diffusion. Our comparative slab data (Table 1) reveal smaller carbon-induced facilitation of the subsurface hydrogen diffusion on the laterally rigid Pd(111) surface. Based on higher barriers of carbon subsurface diffusion on Pd(111) terraces than on near-edge sites of PdNPs,[8] only a limited enhancement of subsurface hydrogen diffusion by co-adsorbed carbon is expected on the extended Pd(111) surface compared to PdNPs. Subsurface carbon in Pd_{79} is calculated to notably alter positions of palladium atoms in the second coordination sphere as well, causing elongation of some Pd–Pd distances involving the next-nearest neighbors to carbon by up to about 10 pm. Thus, not only the surface palladium layers of (111) facets are made strongly more permeable by subsurface carbon for the penetration of hydrogen, but this effect extends in a noticeable size to the subsurface palladium layer and probably also to the layer beneath it, thus assisting in the hydrogen diffusion into the metal bulk.

In summary, we have shown that carbon species can dramatically enhance the rate of hydrogen subsurface diffusion in PdNPs by lowering the activation barrier, which can account for the experimentally observed unusual promotion of sustained hydrogenation activity. Our calculations reveal that this enhancement arises partly from notable destabilization of surface hydrogen atoms on PdNPs in the presence of carbon, and, more importantly, from carbon-induced expansion of the surface openings for penetration of hydrogen into subsurface region. The latter process is accompanied by a strong reduction or elimination of the activation barriers. Our data demonstrate conceptual importance of the atomic flexibility of sites near particle edges that, in contrast to intrinsically rigid regular single crystal surfaces, plays a crucial role in hydrogen subsurface diffusion on palladium.

Experimental Section

The DF calculations were performed with the help of plane-wave VASP[11] code using local density (LDA; VWN exchange-correlation functional[12]) and generalized gradient (GGA; RPBE functional[13]) approximations. Basis sets with kinetic energy of plane waves up to 415 eV were employed. The effect of the $Pd\,1s^2$–$4p^6$ and $C\,1s^2$ core electrons on the valence electron density was accounted for by the projector-augmented wave (PAW) method.[14] A $5\times5\times1$ k-point grid was used for the models based on the six-layer Pd(111) slab with a 3×3 surface unit cell; calculations of a Pd_{79} nanoparticle and complexes of H and C on it were carried out at the Γ point. Interactions of H atoms with pristine and C-covered Pd_{79} clusters were calculated for the fully optimized structures; only in the slab models were Pd atoms of the lowest two layers kept fixed at the experimentally determined positions. The geometric relaxation was stopped when all remaining forces acting on atoms were less than $0.015\ eV\,Å^{-1}$. Transition states were searched in a point-wise fashion along the path connecting adsorption and absorption configurations at fixed heights of the H atom over the nearby surface Pd_3 moiety. The structures near the TS were refined by a quasi-Newton method. The proper character of the adsorption, absorption minima, and of transition states was confirmed by analysis of vibrational frequencies of the H atoms. All binding and activation energies presented above, corrected for the zero-point vibrational energy of H, are calculated in a single-point fashion for the structures optimized at the VWN level using the RPBE functional.[13] In such a way, notable overestimation of Pd–Pd bond lengths in a GGA structural optimization[9,15] and concomitant artificially enhanced permeability of Pd to atomic H is counteracted. Our benchmark calculations using RPBE functional for the structure optimization as well indeed revealed somewhat higher permeability of Pd substrates for H, but all our findings on the subsurface diffusion of H in the presence of C remained the same as obtained in the combined RPBE/VWN description.

Molecular beam experiments were performed at the Fritz-Haber-Institut (Berlin) in a UHV apparatus described in detail previously.[16] An effusive doubly differentially pumped multi-channel array source was used to supply D_2. A supersonic beam, generated by a triply differentially pumped source from a supersonic expansion and modulated by a solenoid valve and a remote-controlled shutter, was used to generate the *cis*-2-butene beam (Aldrich, >99%). An automated quadrupole mass spectrometer system (ABB Extrel) continuously monitored the partial pressure of the reactants (*cis*-2-butene, C_3H_5 fragment detected at 41 a.m.u.) and products ([D_2]butane, $C_3H_5D_2$ fragment at 45 a.m.u.). The QMS data were corrected for the natural abundance of ^{13}C.

The thin (ca. 100 Å) Fe_3O_4 film was grown on a Pt(111) single-crystal by repeated cycles of Fe (>99.99%, Goodfellow) physical vapor deposition and subsequent oxidation (see Refs. [6,17] for details). Pd particles (>99.9%, Goodfellow) were grown by physical vapor deposition using a commercial evaporator (Focus, EFM 3, flux calibrated by a quartz microbalance) with the sample temperature at 115 K. The final Pd coverage was 2.7×10^{15} atoms cm^{-2} and the resulting surface was stabilized via a few cycles of oxygen (8×10^{-7} mbar for 1000 s) and CO exposures (8×10^{-7} mbar for 3000 s) at 500 K.[6] For carbon deposition, two Langmuir ($1\ L = 10^{-6}$ Torr s) *cis*-2-butene were adsorbed on the H (or D)-saturated Pd clusters at 100 K and decomposed by heating to 485 K (see Refs. [4,5] for details).

Received: August 23, 2009
Revised: November 17, 2009
Published online: May 20, 2010

Keywords: carbon · density functional calculations · hydrogenation · metal nanoparticles · surface chemistry

[1] G. C. Bond, *Metal-Catalysed Reactions of Hydrocarbons*, Springer, New York, **2005**.
[2] A. M. Doyle, S. K. Shaikhutdinov, H.-J. Freund, *Angew. Chem.* **2005**, *117*, 635 – 637; *Angew. Chem. Int. Ed.* **2005**, *44*, 629 – 631.
[3] D. Teschner, J. Borsodi, A. Wootsch, Z. Révay, M. Hävecker, A. Knop-Gericke, S. D. Jackson, R. Schlögl, *Science* **2008**, *320*, 86 – 89.
[4] M. Wilde, K. Fukutani, W. Ludwig, B. Brandt, J.-H. Fischer, S. Schauermann, H.-J. Freund, *Angew. Chem.* **2008**, *120*, 9430 – 9434; *Angew. Chem. Int. Ed.* **2008**, *47*, 9289 – 9293.
[5] B. Brandt, J.-H. Fischer, W. Ludwig, J. Libuda, F. Zaera, S. Schauermann, H.-J. Freund, *J. Phys. Chem. C* **2008**, *112*, 11408 – 11420.
[6] T. Schalow, B. Brandt, D. E. Starr, M. Laurin, S. Schauermann, S. K. Shaikhutdinov, J. Libuda, H.-J. Freund, *Catal. Lett.* **2006**, *107*, 189 – 196.
[7] I. V. Yudanov, A. V. Matveev, K. M. Neyman, N. Rösch, *J. Am. Chem. Soc.* **2008**, *130*, 9342 – 9352.
[8] F. Viñes, C. Loschen, F. Illas, K. M. Neyman, *J. Catal.* **2009**, *266*, 59 – 63.
[9] I. V. Yudanov, R. Sahnoun, K. M. Neyman, N. Rösch, *J. Chem. Phys.* **2002**, *117*, 9887 – 9896.
[10] F. Viñes, A. Desikusumastuti, T. Staudt, A. Görling, J. Libuda, K. M. Neyman, *J. Phys. Chem. C* **2008**, *112*, 16539 – 16549.
[11] G. Kresse, J. Furthmüller, *Phys. Rev. B* **1996**, *54*, 11169 – 11186.
[12] S. H. Vosko, L. Wilk, M. Nusair, *Can. J. Phys.* **1980**, *58*, 1200 – 1211.
[13] B. Hammer, L. B. Hansen, J. K. Nørskov, *Phys. Rev. B* **1999**, *59*, 7413 – 7421.
[14] P. E. Blöchl, *Phys. Rev. B* **1994**, *50*, 17953 – 17979.
[15] F. Viñes, F. Illas, K. M. Neyman, *Angew. Chem.* **2007**, *119*, 7224 – 7227; *Angew. Chem. Int. Ed.* **2007**, *46*, 7094 – 7097.
[16] J. Libuda, I. Meusel, J. Hartmann, H.-J. Freund, *Rev. Sci. Instrum.* **2000**, *71*, 4395 – 4408.
[17] C. Lemire, R. Meyer, V. Henrich, S. K. Shaikhutdinov, H.-J. Freund, *Surf. Sci.* **2004**, *572*, 103 – 114.

